Mixed two- and three-photon absorption in bulk rutile (TiO$_2$) around 800 nm

Christopher C. Evans,[1] Jonathan D. B. Bradley,[1] Erwin A. Martí-Panameño,[2] and Eric Mazur[1,*]

[1]*School of Engineering and Applied Sciences, Harvard University, 9 Oxford Street, Cambridge, Massachusetts 02138, USA*
[2]*FCFM, Benemérita Universidad Autónoma de Puebla, Av. San Claudio y Rio Verde, C.P. 72570, Puebla, Puebla, México*
[*]*mazur@seas.harvard.edu*

Abstract: We observe mixed two- and three-photon absorption in bulk rutile (TiO$_2$) around 800 nm using the open aperture Z-scan technique. We fit the data with an extended model that includes multiphoton absorption, beam quality, and ellipticity. The extracted two- and three-photon absorption coefficients are below 1 mm/GW and 2 mm^3/GW^2, respectively. We observe negligible two-photon absorption for 813-nm light polarized along the extraordinary axis. We measure the nonlinear index of refraction and obtain two-photon nonlinear figures of merit greater than 1.1 at 774 nm and greater than 12 at 813 nm. Similarly, we obtain three-photon figures of merit that allow operational intensities up to 0.57 GW/mm^2. We conclude that rutile is a promising material for all-optical switching applications around 800 nm.

©2012 Optical Society of America

References and links

1. R. Adair, L. L. Chase, and S. A. Payne, "Nonlinear refractive index of optical crystals," Phys. Rev. B Condens. Matter **39**(5), 3337–3350 (1989).
2. M. Jinno and T. Matsumoto, "Nonlinear Sagnac interferometer switch and its applications," IEEE J. Quantum Electron. **28**(4), 875–882 (1992).
3. M. A. Foster, A. C. Turner, R. Salem, M. Lipson, and A. L. Gaeta, "Broad-band continuous-wave parametric wavelength conversion in silicon nanowaveguides," Opt. Express **15**(20), 12949–12958 (2007).
4. G. I. Stegeman and W. E. Torruellas, "Nonlinear materials for information processing and communications," Philos. Trans. R. Soc. Lond. A **354**(1708), 745–756 (1996).
5. M. Sheik-Bahae, D. J. Hagan, and E. W. Van Stryland, "Dispersion and band-gap scaling of the electronic Kerr effect in solids associated with two-photon absorption," Phys. Rev. Lett. **65**(1), 96–99 (1990).
6. E. W. Van Stryland, M. A. Woodall, H. Vanherzeele, and M. J. Soileau, "Energy band-gap dependence of two-photon absorption," Opt. Lett. **10**(10), 490–492 (1985).
7. J. Pascual, J. Camassel, and H. Mathieu, "Fine structure in the intrinsic absorption edge of TiO$_2$," Phys. Rev. B **18**(10), 5606–5614 (1978).
8. Y. Watanabe, M. Ohnishi, and T. Tsuchiya, "Measurement of nonlinear absorption and refraction in titanium dioxide single crystal by using a phase distortion method," Appl. Phys. Lett. **66**(25), 3431–3432 (1995).
9. A. Penzkofer and W. Falkenstein, "Direct determination of the intensity of picosecond light pulses by two-photon absorption," Opt. Commun. **17**(1), 1–5 (1976).
10. H. S. Waff and K. Park, "Structure in the two-photon absorption spectrum of TiO$_2$ (Rutile)," Phys. Lett. A **32**(2), 109–110 (1970).
11. P. Sathy and A. Penzkofer, "Three-photon absorption and its limitation of third-order nonlinear optical effects in rutile," Appl. Phys. B **61**(2), 127–134 (1995).
12. K. Watanabe, K. Inoue, and F. Minami, "Resonant phenomena of hyper-Raman-scattering of optic phonons in a TiO$_2$ crystal," Phys. Rev. B Condens. Matter **46**(4), 2024–2033 (1992).
13. T. Hashimoto, T. Yoko, and S. Sakka, "Sol-gel preparation and third-order nonlinear optical properties of TiO$_2$ thin films," Bull. Chem. Soc. Jpn. **67**(3), 653–660 (1994).
14. H. Long, A. Chen, G. Yang, Y. Li, and P. Lu, "Third-order optical nonlinearities in anatase and rutile TiO$_2$ thin films," Thin Solid Films **517**(19), 5601–5604 (2009).
15. D. Torres-Torres, M. Trejo-Valdez, L. Castañeda, C. Torres-Torres, L. Tamayo-Rivera, R. C. Fernández-Hernández, J. A. Reyes-Esqueda, J. Muñoz-Saldaña, R. Rangel-Rojo, and A. Oliver, "Inhibition of the two-

photon absorption response exhibited by a bilayer TiO$_2$ film with embedded Au nanoparticles," Opt. Express **18**(16), 16406–16417 (2010).

16. M. Trejo-Valdez, R. Torres-Martínez, N. Peréa-López, P. Santiago-Jacinto, and C. Torres-Torres, "Contribution of the two-photon absorption to the third order nonlinearity of au nanoparticles embedded in TiO$_2$ films and in ethanol suspension," J. Phys. Chem. C **114**(22), 10108–10113 (2010).
17. H. Long, G. Yang, A. Chen, Y. Li, and P. Lu, "Femtosecond Z-scan measurement of third-order optical nonlinearities in anatase TiO$_2$ thin films," Opt. Commun. **282**(9), 1815–1818 (2009).
18. M. Kyoung and M. Lee, "Z-scan studies on the third-order optical nonlinearity of Au nanoparticles embedded in TiO$_2$," Bull. Korean Chem. Soc. **21**, 26–28 (2000).
19. H. I. Elim, W. Ji, A. H. Yuwono, J. M. Xue, and J. Wang, "Ultrafast optical nonlinearity in poly(methylmethacrylate)-TiO$_2$ nanocomposites," Appl. Phys. Lett. **82**(16), 2691–2693 (2003).
20. L. Irimpan, B. Krishnan, V. P. N. Nampoori, and P. Radhakrishnan, "Luminescence tuning and enhanced nonlinear optical properties of nanocomposites of ZnO-TiO$_2$.," J. Colloid Interface Sci. **324**(1-2), 99–104 (2008).
21. A. H. Yuwono, B. Liu, J. Xue, J. Wang, H. I. Elim, W. Ji, Y. Li, and T. J. White, "Controlling the crystallinity and nonlinear optical properties of transparent TiO$_2$-PMMA nanohybrids," J. Mater. Chem. **14**(20), 2978–2987 (2004).
22. Q. F. Zhou, Q. Q. Zhang, J. X. Zhang, L. Y. Zhang, and X. Yao, "Preparation and optical properties of TiO$_2$ nanocrystalline particles dispersed in SiO$_2$ nano-composites," Mater. Lett. **31**(1-2), 39–42 (1997).
23. M. Sheik-Bahae, A. A. Said, T. H. Wei, D. J. Hagan, and E. W. Van Stryland, "Sensitive measurement of optical nonlinearities using a single beam," IEEE J. Quantum Electron. **26**(4), 760–769 (1990).
24. M. Higuchi, T. Hosokawa, and S. Kimura, "Growth of rutile single crystals by floating zone method," J. Cryst. Growth **112**(2-3), 354–358 (1991).
25. E. W. V. Stryland and M. Sheik-Bahae, "Z-Scan measurements of optical nonlinearities," in *Characterization techniques and tabulations for organic nonlinear optical materials*, M. G. Kuzyk and C. W. Dirk, eds. (Marcel Dekker, 1998).
26. S. Couris, M. Renard, O. Faucher, B. Lavorel, R. Chaux, E. Koudoumas, and X. Michaut, "An experimental investigation of the nonlinear refractive index (n$_2$) of carbon disulfide and toluene by spectral shearing interferometry and z-scan techniques," Chem. Phys. Lett. **369**(3-4), 318–324 (2003).
27. R. A. Ganeev, A. I. Ryasnyansky, M. Baba, M. Suzuki, N. Ishizawa, M. Turu, S. Sakakibara, and H. Kuroda, "Nonlinear refraction in CS$_2$," Appl. Phys. B **78**(3-4), 433–438 (2004).
28. M. Falconieri and G. Salvetti, "Simultaneous measurement of pure-optical and thermo-optical nonlinearities induced by high-repetition-rate, femtosecond laser pulses: application to CS$_2$," Appl. Phys. B **69**(2), 133–136 (1999).
29. A. Gnoli, L. Razzari, and M. Righini, "Z-scan measurements using high repetition rate lasers: how to manage thermal effects," Opt. Express **13**(20), 7976–7981 (2005).
30. B. M. Patterson, W. R. White, T. A. Robbins, and R. J. Knize, "Linear optical effects in z-scan measurements of thin films," Appl. Opt. **37**(10), 1854–1857 (1998).
31. D. S. Corrêa, L. De Boni, L. Misoguti, I. Cohanoschi, F. E. Hernandez, and C. R. Mendonça, "Z-scan theoretical analysis for three-, four- and five-photon absorption," Opt. Commun. **277**(2), 440–445 (2007).
32. K. Watanabe and K. Inoue, "Two-photon resonant effect of hyper-Raman scattering in the vicinity of the direct forbidden gap in a rutile crystal," Phys. Rev. B Condens. Matter **41**(11), 7957–7960 (1990).
33. C. C. Evans, J. D. B. Bradley, F. Parsy, K. C. Phillips, R. Senaratne, E. A. Martí-Panameño, and E. Mazur, "Thermally managed Z-scan measurements of titanium dioxide thin films," presented at Photonics West, San Francisco, CA, USA, 27 Jan. 2011.
34. B. Imangholi, M. P. Hasselbeck, and M. Sheik-Bahae, "Absorption spectra of wide-gap semiconductors in their transparency region," Opt. Commun. **227**(4-6), 337–341 (2003).
35. J. Yao, Z. Fan, Y. Jin, Y. Zhao, H. He, and J. Shao, "Investigation of damage threshold to TiO$_2$ coatings at different laser wavelength and pulse duration," Thin Solid Films **516**(6), 1237–1241 (2008).
36. M. Mero, J. Liu, W. Rudolph, D. Ristau, and K. Starke, "Scaling laws of femtosecond laser pulse induced breakdown in oxide films," Phys. Rev. B **71**(11), 115109 (2005).
37. V. G. Ta'eed, N. J. Baker, L. B. Fu, K. Finsterbusch, M. R. E. Lamont, D. J. Moss, H. C. Nguyen, B. J. Eggleton, D. Y. Choi, S. Madden, and B. Luther-Davies, "Ultrafast all-optical chalcogenide glass photonic circuits," Opt. Express **15**(15), 9205–9221 (2007).
38. S. J. Madden, D. Y. Choi, D. A. Bulla, A. V. Rode, B. Luther-Davies, V. G. Ta'eed, M. D. Pelusi, and B. J. Eggleton, "Long, low loss etched As$_{(2)}$S$_{(3)}$ chalcogenide waveguides for all-optical signal regeneration," Opt. Express **15**(22), 14414–14421 (2007).
39. I. D. Rukhlenko, M. Premaratne, and G. P. Agrawal, "Analytical study of optical bistability in silicon ring resonators," Opt. Lett. **35**(1), 55–57 (2010).
40. P. Koonath, D. R. Solli, and B. Jalali, "Limiting nature of continuum generation in silicon," Appl. Phys. Lett. **93**(9), 091114 (2008).
41. B. Gu, J. Wang, J. Chen, Y.-X. Fan, J. Ding, and H.-T. Wang, "Z-scan theory for material with two- and three-photon absorption," Opt. Express **13**(23), 9230–9234 (2005).
42. B. Gu, X. Q. Huang, S. Q. Tan, M. Wang, and W. Ji, "Z-scan analytical theories for characterizing multiphoton absorbers," Appl. Phys. B **95**(2), 375–381 (2009).
43. J. Wang, B. Gu, X.-W. Ni, and H.-T. Wang, "Z-scan theory with simultaneous two- and three-photon absorption saturation," Opt. Laser Technol. **44**(2), 390–393 (2012).
44. S. M. Mian, B. Taheri, and J. P. Wicksted, "Effects of beam ellipticity on Z-scan measurements," J. Opt. Soc. Am. B **13**(5), 856–863 (1996).

45. M. G. Vivas, T. Shih, T. Voss, E. Mazur, and C. R. Mendonca, "Nonlinear spectra of ZnO: reverse saturable, two- and three-photon absorption," Opt. Express **18**(9), 9628–9633 (2010).
46. G. Boudebs, S. Cherukulappurath, M. Guignard, J. Troles, F. Smektala, and F. Sanchez, "Experimental observation of higher order nonlinear absorption in tellurium based chalcogenide glasses," Opt. Commun. **232**(1-6), 417–423 (2004).
47. M. Chattopadhyay, P. Kumbhakar, C. S. Tiwary, A. K. Mitra, U. Chatterjee, and T. Kobayashi, "Three-photon-induced four-photon absorption and nonlinear refraction in ZnO quantum dots," Opt. Lett. **34**(23), 3644–3646 (2009).
48. T. Sarma, P. K. Panda, P. T. Anusha, and S. V. Rao, "Dinaphthoporphycenes: synthesis and nonlinear optical studies," Org. Lett. **13**(2), 188–191 (2011).
49. P. B. Chapple, J. Staromlynska, J. A. Hermann, T. J. McKay, and R. G. McDuff, "Single-beam Z-scan: measurement techniques and analysis," J. Nonlinear Opt. Phys. Mater. **6**(3), 251–293 (1997).
50. A. Eriksson, M. Lindgren, S. Svensson, and P.-O. Arntzen, "Numerical analysis of Z-scan experiments by use of a mode expansion," J. Opt. Soc. Am. B **15**(2), 810–816 (1998).
51. I. O. f. Standardization, ISO 11146–1:2005 Lasers and laser-related equipment - Test methods for laser beam widths, divergence angles and beam propagation ratios (Geneva, Switzerland, 2005).

1. Introduction

Rutile (titanium dioxide) is a wide-bandgap semiconductor, advantageous for many optical applications due to its high refractive index, birefringence, and transparency for wavelengths ≥ 400 nm. In addition, it is naturally abundant, and highly stable. Rutile also has a large Kerr nonlinearity ($n_2 = 9 \times 10^{-19}$ m^2/W) [1]. These properties make rutile a promising material for nonlinear all-optical applications such as ultrafast switching, logic [2] and wavelength conversion [3].

Even with a high Kerr nonlinearity, two- and three-photon absorption (2PA and 3PA, respectively) impose limitations for nonlinear optical devices that rely on high intensities [4]. For semiconductors, we expect 2PA (3PA) to occur for photon energies equal to or greater than the half- (third-) bandgap energy (E_g) [5, 6]. The half- (third-) bandgap energy corresponds to 800 nm (1200 nm) in rutile ($E_g = 3.101$ eV) [7]. We expect device properties to be strongly wavelength dependent around 800 nm due to the transition from pure 3PA to mixed two- and three-photon absorption.

Studies have quantified pure 2PA in bulk rutile for visible wavelengths (532–750 nm) [8–10] and 3PA for near-infrared wavelengths (1054 μm) [11]. In bulk rutile, two-photon absorption was observed via weak luminescence for pump wavelengths near 800 nm, however two-photon absorption coefficients were not reported [12]. Meanwhile, the nonlinear properties of TiO$_2$ films [13–20] and TiO$_2$ composites [15, 16, 18, 19, 21, 22] have been extensively investigated. Of these thin film studies, those that address pure-phase TiO$_2$ near 800 nm report effective two-photon absorption coefficients that vary in both magnitude and sign [14, 15, 17–20]. However, there are no reports on two-photon absorption in the bulk material using similar laser parameters for comparison. In addition, 3PA near 800 nm in bulk rutile has not been reported. Therefore, our understanding of multiphoton absorption in bulk rutile is incomplete and requires further study around 800 nm.

In this paper, we investigate multiphoton absorption near 800 nm in bulk rutile using the open aperture Z-scan technique [23]. We develop a theoretical model to fit the experimental data and extract two- and three-photon absorption coefficients for different wavelengths and crystal orientations. Using the extracted multiphoton absorption coefficients, we discuss nonlinear absorption processes near rutile's half-bandgap and evaluate its applicability as a material for all-optical devices.

2. Experimental

We perform open-aperture Z-scan measurements using two commercially available 1-mm-thick single-crystal rutile samples grown using the floating zone method [24]. One sample is cleaved along the (001) plane and the second is cleaved along the (100) plane. The (001)-cut allows for measurements with the incident laser beam polarized along the ordinary axis of the crystal ($E \perp c$), while the (100)-cut allows for polarization along both the ordinary and extraordinary axes ($E \parallel c$).

Our experimental setup is similar to that described in [23]. We use a chirped-pulse amplified Ti:Sapphire system with pulse durations $\tau \geq 50$ fs, energies up to 3 µJ at a repetition rate of 250 kHz. We measure the pulse duration using frequency-resolved optical gating (FROG). The beam is spatially filtered to obtain a Gaussian shape then focused through a lens with a 0.15-m focal length. A scanning slit detector on a single axis stage measures the caustic (beam width versus z-position). The caustic determines the beam waist (w_{0x}, w_{0y} in the x and y directions, respectively), quality factor (M^2) and ellipticity (w_{0x}/w_{0y}). A reference detector before the lens allows us account for small power fluctuations [25]. We adjust the central wavelengths, λ_0, of the fs-pulses by spectrally filtering the seed using a physical aperture within the pulse-stretcher before the amplifier. Without filtering, the spectral width, $\Delta\lambda$ (FWHM), is 30 nm at $\lambda_0 = 800$ nm with a pulse duration of 50 fs. With filtering, we obtain narrow-band spectra centered at either 774 nm or 813 nm with spectral widths of 4 and 10 nm, respectively. Table 1 presents a summary of the measured laser parameters.

We carry out a set of open-aperture Z-scan measurements at the three different central wavelengths for each sample/orientation. Each measurement set consists of five different Z-scan curves for different incident powers. Measurements taken at low irradiances (< 0.06 GW/mm^2) characterize linear signal caused by sample imperfections. We use this signal to remove the linear response from the four higher-power measurements [23].

Table 1. Measured Laser Parameters*

λ_0 (nm)	$2\hbar\omega$ (eV)	$\Delta\lambda$ (nm)	τ (fs)	$w_{0,\text{ave}}$ (µm)	$z_{0,\text{av}}$ (mm)	M^2	w_{x0}/w_{y0}	$I_{0,\text{max}}$ (GW/mm^2)
774	3.20	4	290	33	4.4	< 1.13	0.78	0.21
813	3.05	10	174	36	5.0	< 1.18	0.92	0.32
800	3.10	30	50	28	3.1	< 1.06	0.95	1.04

*Measured laser parameters for measurements taken at spectrally filtered center wavelengths of 774 and 813 nm as well as unfiltered measurements at 800 nm. Here, λ_0 is the center wavelength, $2\eta\omega$ is the two-photon energy, $\Delta\lambda$ is the measured bandwidth (full-width at half-maximum), τ is the pulse duration, $w_{0,\text{ave}}$ is the average beam waist, $z_{0,\text{ave}}$ is the average Rayleigh distance, M^2 is the beam parameter product, w_{x0}/w_{y0} is the ellipticity and $I_{0,\text{max}}$ is maximum peak on-axis irradiance for the highest power measurement used for analysis.

The intensity dependent attenuation coefficient is approximately given by $\alpha(I, \lambda) = \alpha_0 + \alpha_2 I + \alpha_3 I^2$, where I is the intensity, α_0 is the linear attenuation coefficient ($\alpha_0 \approx 0$ for $\lambda = 800$ nm in rutile), α_2 is the 2PA coefficient, and α_3 is the 3PA coefficient. These coefficients are wavelength dependent. We extract multiphoton absorption coefficients by numerically fitting the measured data to a theoretical model that takes into account the experimental beam and sample parameters (see Appendix A). Our mixed multiphoton absorption model has four degrees of freedom (α_2, α_3, waist position, and astigmatism). Using this model, we fit the multiple Z-scan curves taken at different peak irradiances simultaneously to extract a single value of α_2 and α_3 for a given wavelength and polarization.

3. Results and discussion

3.1 Open aperture Z-scan measurements

We show open aperture Z-scan measurements of bulk rutile for different incident wavelengths and pulse durations in Figs. 1 through 4. Figure 1 (left) shows a typical experimental open aperture Z-scan curve in rutile for 800-nm, 50-fs pulses with $E \| c$. Figure 1 (right) shows the transmittance change ($\Delta T = 1 - T$, at the focus) as a function of the peak on-axis irradiance for the same sample and pulse duration (referred to here as a ΔT-plot). Figure 2 shows data collected using $\lambda_0 = 774$ nm and an input beam polarized with $E \perp c$ and $E \| c$ (Figs. 2, left and

right, respectively). Similarly, Figs. 3 and 4 show measurements and fits for $\lambda_0 = 813$ nm and $\lambda_0 = 800$, respectively.
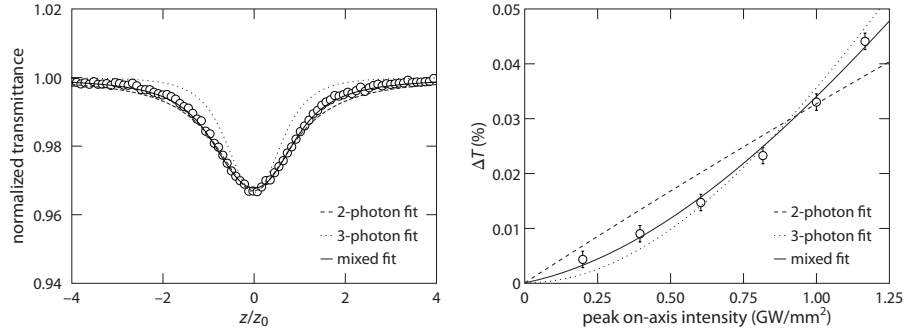

Fig. 1. The left plot shows open-aperture Z-scan measurements of bulk rutile (open circles) using a 50-fs pulse with $\lambda_0 = 800$ nm for the extraordinary ($E \| c$) polarization (peak on-axis irradiance of 0.95 GW/mm^2). Theoretical fits for pure two-photon [23], three-photon [31], and our mixed multi-photon absorption models are shown in dashed, dotted, and solid lines, respectively. The right plot shows the change in transmittance ($\Delta T = 1 - T$) at the focus as a function of peak on-axis irradiance for the same sample, wavelength, and pulse duration. Data is shown in open circles with error bars. Theoretical fits for pure two-photon, three-photon and mixed two- and three-photon absorption are shown in dashed, dotted, and solid lines, respectively.

The primary sources of uncertainty in our Z-scan measurements are the noise of the laser and sample imperfections. We measure laser noise to be ±1–2%. Using low intensity and by adjusting the sample position, we reduce the linear background variations caused by sample imperfections to less than 1%. To reduce the overall noise, we use a reference photodiode, drift detection, temporal averaging, and background subtraction. These methods suppress the normalized transmittance variation to ±0.0015. Consecutive scans resulted in measurements that were within this transmittance variation. To characterize the repeatability of our technique, we analyzed four measurement sets using $E \perp c$, taken over non-consecutive days for both the (001)- and (100)-cut. We could not compare these measurements on a point-for-point basis, consequently, we analyzed these measurement sets using our mixed two- and three-photon model (see Appendix A) and determined the standard deviation of α_2 and α_3. We obtain a standard deviation of 5% for α_2 and 18% for α_3. In addition, we have tested our system using CS_2 with a 50-fs pulse at 800 nm and we obtain a 2PA coefficient of 0.06 mm/GW using standard analysis. This value falls within the range of values obtained for CS_2 in previous studies using 110-fs pulses [26, 27] and thermal methods [28, 29].

Sample damage [30] and thermal effects [28, 29] can mask electronic nonlinearities. We verified that no damage or alterations occurred to the sample by comparing low irradiance scans taken directly before and after each high intensity measurement set. We performed thermally managed Z-scan [28, 29] using our bulk rutile samples in both open- and closed-aperture configurations. By utilizing an optical chopper and fast photodiodes to resolve pulse-to-pulse transmittance changes, we did not observe cumulative (i.e. thermal) changes in the signal. Similarly, measurements taken at 10 kHz produced equivalent measurements to those taken at 250 kHz, confirming that no cumulative effects were present.

3.2 Justification and fitting of the mixed-multiphoton absorption model

To establish the optimum fitting procedure, we first fit our data with standard open-aperture Z-scan models and compare to our mixed-multiphoton absorption model. Figure 1 (left) presents a typical experimental Z-scan curve that is fit using a pure 2PA-model [23], a pure 3PA-model [31] and our mixed-multiphoton model (dashed, dotted, and solid lines, respectively). In Fig. 1 (right), we show an experimental ΔT-plot which is fit using a pure 2PA-, 3PA- and our mixed-multiphoton model (dashed, dotted, and solid lines, respectively).

Comparing a pure 2PA to a pure 3PA model, we find that fitting individual Z-scan curves appears to favor the 2PA model. However, a 2PA model predicts a very different ΔT behavior with increasing irradiance. Three-photon absorption better fits the high intensity ΔT data, yet is insufficient for low intensity data and individual Z-scan curves. We see that our mixed-multiphoton model provides an excellent fit to both Z-scan curves and ΔT-plots. These observations highlight two important points. First, neither a pure 2PA- nor a pure 3PA-model can describe the data sufficiently, necessitating a mixed-multiphoton absorption model. Second, both curve fitting and the ΔT-plot method provide complimentary information. Curve fitting is advantageous because signal away from the focus always contains the lowest order absorption, such as 2PA. However, curve fitting can mask higher order absorption and is susceptible to beam distortions. In contrast, the ΔT-plot provides a fast measure on higher order absorption processes. Yet, this method may overlook lower order absorption if sufficient low irradiance data is not included.

Quantifying mixed two- and three-photon absorption requires a balance between the curve fitting and the ΔT-plot methods. It also requires further constraint to account for the additional fitting coefficients. Consequently, we use a more robust method whereby we fit an entire measurement set, consisting of several full Z-scan curves taken at different peak irradiances, using a single set of parameters. This technique produces equivalent results to the ΔT-plot method within the uncertainty.

We tested the optimization algorithm by using various starting points while keeping all other parameters at experimentally determined values. These variations included starting both α_2 and α_3 at zero as well as other magnitudes and signs of α_2, α_3 and the astigmatism. Other combinations, such as two- and four-photon absorption (with astigmatism) could produce reasonable fits in some, but not all cases (notably the 813-nm data set). We found that including two- and three-photon absorption in our model resulted in good fits for all experimental data while minimizing the number of fitted parameters.

We quantitatively compare the fit quality using standard 2PA [23] and 3PA [31] models to our mixed-multiphoton model. Fitting a full data set (for example, a 50 fs pulse, $E\|c$) using a 2PA or 3PA model produces R^2 values of 0.974 and 0.925 for ± 4 Rayleigh distance (respectively). We fit the same data set with our mixed-multiphoton model and observe an R^2 of 0.991 (solid lines, Fig. 4 right). We performed a similar analysis with the 813-nm data set ($E\|c$) and obtain R^2 values of 0.841, 0.944 and 0.950 (2PA, 3PA and mixed-multiphoton models, respectively). From this analysis, the R^2 correlation shows that the mixed-multiphoton model fits the data better than either a pure two- or three-photon absorption model in all cases. Therefore, we conclude that our mixed-multiphoton model is adequate for fitting our experimental data and use this model to fit the Z-scan data in Figs. 2–4 (shown in solid lines).

Two additional fitting parameters were included in the two- and three-photon absorption fitting method. We fit the beam waist location, which aligns the model to the experimental waist position. We found that fitting the astigmatism resulted in a significant improvement in fit quality that we could not achieve by other means (i.e. using additional multiphoton absorption terms or fitting the waist). However, the fit astigmatism is relatively large, ranging from 25% to 100% of the measured Rayleigh distance. We find the largest fit astigmatism using 50-fs pulses. Meanwhile, the measured astigmatism is only up to 12% of the Rayleigh distance. This discrepancy represents the largest source of uncertainty within our analysis. By including the effects of fitting with and without the astigmatism, we estimate the uncertainty to be ± 15% in α_2 and a factor of 2 for α_3.

3.3 Two- and three-photon absorption coefficients

Table 2 summarizes bulk rutile two- and three-photon absorption coefficients. Overall, α_2 ranges from less than 10^{-7} mm/GW to 0.9 mm/GW (± 15%). Comparing 774 nm to 813 nm measurements, we find that the 2PA coefficients at these two wavelengths differ considerably. At 774 nm, α_2 is 0.54 mm/GW ($E\perp c$) and 0.89 mm/GW ($E\|c$). At 813 nm and $E\|c$, α_2 is below the measureable limit. For $E\perp c$, we extract a value of 0.08 mm/GW. Lastly, two-

photon absorption coefficients for 800 nm are between the 774 nm and 813 nm coefficients. Rutile has typical values of α_3 on the order of 1 mm^3/GW^2 as shown in Table 2. The values of α_3 at 800 nm are 0.2 mm^3/GW^2. We observe 4 to 9 times higher three-photon absorption coefficients for 774 and 813 nm wavelengths. The difference in α_3 between 774-nm and 813-nm measurements is less than a factor of two and is therefore within the experimental uncertainty (considering both orientations).
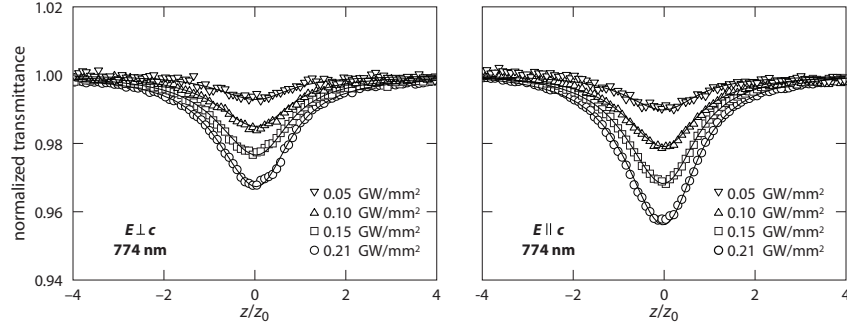
Fig. 2. Open-aperture Z-scan measurements of bulk rutile using a 290-fs pulse with $\lambda_0 = 774$ nm for ordinary ($E \perp c$) and extraordinary ($E \| c$) polarizations (left and right, respectively). Solid lines are a fit across all irradiances shown. Fit parameters are α_2, α_3, average z_0 and the astigmatism.

These values of α_2 and α_3 in bulk rutile are consistent with values obtained under similar conditions [11]. Our degenerate 2PA coefficients around 774 nm are in good agreement with other nondegenerate two-photon absorption measurements (using a 1054-nm pump and a 612-nm probe producing an effective α_2 coefficient of 1–5 mm/GW) [11]. Similarly, our values of α_3 (0.2–2 mm^3/GW^2) are within the range of measurements taken at 1054 nm (0.5 mm^3/GW^2) in the same study.

Recently, both negative and positive 2PA coefficients of significantly higher magnitude have been measured in TiO$_2$ thin films in the 750–830 nm range [14, 15, 17–19]. However, the thin films investigated vary widely in growth methods, composition, and crystalline phase, thus making it difficult to compare directly to the bulk measurements reported here. Furthermore, while our values are consistent with other bulk measurements, there are inconsistencies with reported thin film values in both sign and magnitude for polycrystalline rutile [14] and anatase TiO$_2$ [14, 15, 18, 19]. Thin films are more challenging to measure than bulk samples, and often require intensities approaching the damage threshold to achieve sufficient signal-to-noise, which may lead to linear effects that appear as nonlinear signal [30]. Therefore, further investigation of TiO$_2$ thin film versus bulk nonlinearities is required.

We find that the 2PA coefficients decrease significantly between 774 and 813 nm. These wavelengths correspond to two-photon energies of $2\hbar\omega = 3.20$ eV and 3.05 eV, respectively. These two-photon energies lie on opposite sides of rutile's indirect bandgap (3.101 eV) [7]. Although we observe no effective 2PA for $E\|c$ at 813 nm, we still measure a small 2PA-signal for $E \perp c$. Other studies attribute weak absorption at 3.062 eV, which is only present for $E \perp c$, to a direct forbidden bandgap [7, 12, 32]. This energy is within the two-photon bandwidth of the 813-nm pulse and is likely the cause of the small 2PA-signal observed. Between these two effects, the resonance at rutile's indirect bandgap is the largest source of 2PA. This analysis implies that using wavelengths further red-shifted from the two-photon resonance (longer than 800 nm) should result in reduced 2PA.
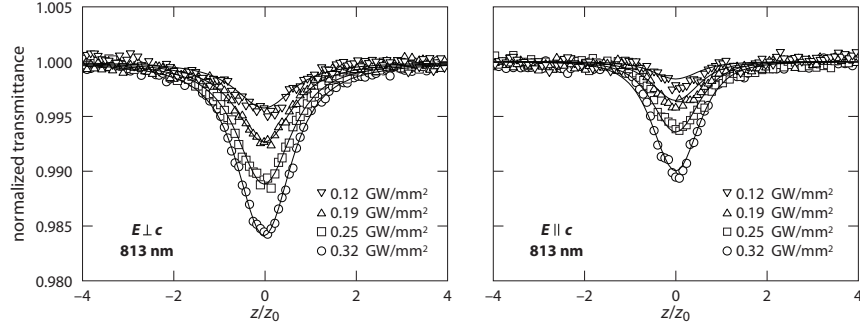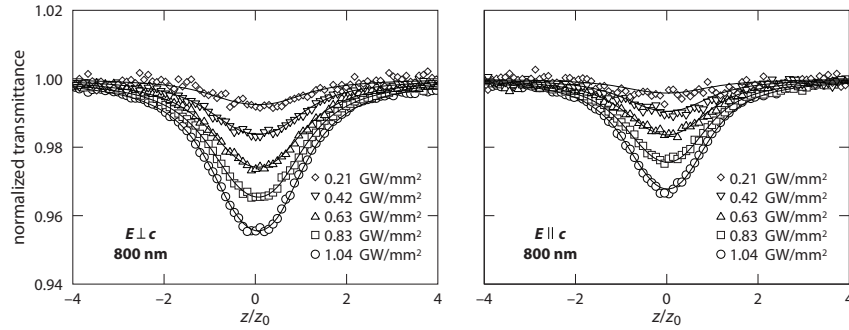
Fig. 3. Open-aperture Z-scan measurements of bulk rutile using a 174-fs pulse with $\lambda_0 = 813$ nm for ordinary ($E \perp c$) and extraordinary ($E \| c$) polarizations (left and right, respectively). Solid lines are a fit across all intensities shown. Fit parameters are α_2, α_3, average z_0 and the astigmatism.

Fig. 4. Open-aperture Z-scan measurements of bulk rutile using a 50-fs pulse with $\lambda_0 = 800$ nm for ordinary ($E \perp c$) and extraordinary ($E \| c$) polarizations (left and right, respectively). Solid lines are a fit across all intensities shown. Fit parameters are α_2, α_3, average z_0 and the astigmatism.

The measurements at 800 nm using a 50-fs pulse require additional interpretation. We find the 2PA coefficients using 800-nm light lie between the values obtained at 774 nm and 813 nm. As shown in Table 2, as the wavelength increases, α_2 decreases monotonically as it passes through the two-photon resonance at the band-edge. This behavior at 800 nm may be partially due to the pulse's extended spectrum (785–815 nm, FWHM). This bandwidth includes spectral components experiencing both higher (774 nm, $\Delta\lambda = 4$ nm) and lower (813 nm, $\Delta\lambda = 10$ nm) 2PA. This implies that the extracted values of α_2 are a convolution between the pulse spectrum and the two-photon absorption spectrum.

We also observe that the three-photon absorption coefficients measured using a 50-fs pulse are 4–10 times smaller than for either 774 or 813 nm. This reduction is unexpected given that the 3PA coefficients do not change significantly between these wavelengths. This reduction is likely due to the model not taking dispersive and nonlinear pulse broadening into account. In the normal group velocity dispersion-regime, with rutile's positive n_2, a pulse broadens temporally during propagation. This broadening decreases the peak intensity and leads to reduced multiphoton absorption. Dispersive broadening is significant if the dispersion length is shorter than or comparable to the sample length. Using the group velocity dispersion for rutile's extraordinary axis ($\beta_2 = 1250$ fs^2/mm) and a pulse duration of $\tau = 50$ fs, we calculate a dispersion length of $\tau^2/\beta_2 = 2$ mm, reducing the peak intensity by 40% over the sample length. In contrast, pulse broadening is negligible for a 174-fs (290-fs) pulse where the dispersion length is 2.4 cm (6.7 cm), resulting in a peak reduction of less than 1%. This intensity reduction has a more pronounced effect on 3PA than on 2PA owing to the I^3- versus I^2-dependence. Taking dispersion into account, the uncertainty in the 800-nm measurements

increases to $\pm 80\%$ in α_2 and a factor of 6 for α_3. Because of the large uncertainty introduced by both dispersive and spectral convolution effects at shorter pulse durations, it is difficult to draw strong conclusions on the time-dependence of nonlinear processes in rutile using the present analysis.

Table 2. Nonlinear Absorption Coefficients, 2PA Figures of Merit and Maximum Intensities from 3PA*

λ_0 (nm)	$2\hbar\omega$ (eV)	ordinary polarization ($E \perp c$)				extraordinary polarization ($E \| c$)			
		α_2 (mm/GW)	α_3 (mm^3/GW^2)	$\dfrac{n_2}{\alpha_2\lambda}$	I_{max}^{3PA} (GW/mm^2)	α_2 (mm/GW)	α_3 (mm^3/GW^2)	$\dfrac{n_2}{\alpha_2\lambda}$	I_{max}^{3PA} (GW/mm^2)
774	3.20	0.54	1.1	1.9	0.93	0.89	1.8	1.1	0.57
813	3.05	0.08	0.8	12.1	1.20	$<10^{-7}$	0.9	$>10^6$	1.10
800	3.10	0.15	0.2	6.6	4.90	0.09	0.2	11.0	4.90

*Fitted nonlinear absorption coefficients, calculated 2PA figures of merit and maximum intensities from 3PA (using $n_2 = 7.9 \times 10^{-19}$ m^2/W [33]). Here, λ_0 is the center wavelength, $2\eta\omega$ is the two-photon energy, α_2 is the 2PA coefficient, α_3 is the 3PA coefficient, $n_2/(\alpha_2\lambda)$ is the 2PA figure of merit and I_{max}^{3PA} is the maximum intensity calculated from the 3PA figure of merit, $1 < [n_2/(\alpha_3\lambda I_{max})]$ [4]. The uncertainty for measurements at 774 nm and 813 nm is $\pm 15\%$ for α_2 and a factor of 2 for α_3. For 800 nm, the uncertainty is $\pm 80\%$ for α_2 and a factor of 6 for α_3.

3.4 Nonlinear figures of merit

Multiphoton absorption has important implications for nonlinear optical devices. Material performance is quantified by the nonlinear figures of merit [4]. The 2PA figure of merit (FOM) is given by $n_2/(\alpha_2\lambda)$ and the 3PA FOM is given by $n_2/(\alpha_3\lambda I_{max})$, where I_{max} is the peak operational intensity. Both FOMs should be greater than unity for all-optical applications. By setting the 3PA FOM equal to one, we calculate the intensity at which 3PA becomes a limit, given by $I_{max}^{3PA} = n_2/(\alpha_3\lambda)$. We measured the nonlinear index of refraction around 800-nm (50-fs pulse) using closed-aperture Z-scan and obtain a value of 7.9×10^{-19} m^2/W for both polarizations using standard analysis methods [33]. Although theory predicts a resonant enhancement of the nonlinear index near the half-bandgap [5], we did not measure a significant deviation from values reported at 1064 nm [1], which may be due to dispersive broadening as explained in the previous section. Therefore, the calculated nonlinear figures of merit should be considered a lower limit. Using the nonlinear index and multiphoton absorption coefficients, we evaluate rutile as a candidate material for all-optical applications around 800 nm by calculating its nonlinear figures of merit.

Table 2 shows the calculated 2PA FOMs and I_{max}^{3PA} for each measurement. The 2PA FOMs at 774 nm are the lowest observed (1.9 and 1.1 for $E \perp c$ and $E \| c$, respectively). At 813 nm, we obtain a FOM of 12.1 for $E \perp c$ and greater than 10^6 for $E \| c$. Calculated I_{max}^{3PA} is lowest for $E \| c$ using 774 nm, with a value of 0.57 GW/mm^2, and greater than 0.93 GW/mm^2 for all other measurements.

All 2PA figures of merit calculated are greater than 1.1, which implies that rutile is compatible with all-optical applications. Measurements at 813 nm show extremely large FOMs, which is favorable for devices. We observe that 2PA can be neglected at 813 nm ($E \| c$) and expect similar results for $E \perp c$ at longer wavelengths [34]. These FOMs imply compatibility with popular femtosecond pulsed sources such as Ti:Sapphire and fiber lasers.

Although 2PA may be negligible for certain wavelengths, we must still avoid significant 3PA by operating below I_{max}^{3PA}. For the largest 3PA measured, I_{max}^{3PA} is 0.57 GW/mm^2 ($E \| c$, 774 nm). This limit is far below thin-film damage thresholds for TiO$_2$ [35, 36] and provides a reasonable upper limit for integrated photonic devices [37–40].

4. Conclusion

We observe mixed two- and three-photon absorption in bulk rutile around 800 nm. By fitting open aperture Z-scan data to a numeric model, we separate the effects of mixed multiphoton absorption. Two- and three-photon absorption coefficients are below 1 mm/GW and 2 mm^3/GW^2, respectively. Two-photon absorption falls below our measurement capabilities for 174-fs pulse with a central wavelength of 813 nm (E‖c). We determine 2PA FOMs greater than 1 above and below rutile's half-bandgap. We expect superior performance for $\lambda_0 \geq 813$ nm, where the 2PA FOMs are greater than 12.1. Additionally, 3PA is sufficiently small to enable all-optical applications for intensities below 0.57 GW/mm^2. From the low two- and three-photon absorption, we conclude that rutile TiO$_2$ is a promising material for all-optical applications such as switching and logic near 800 nm.

Appendix A: theoretical model

Several reports of modeling multiphoton absorption using the Z-scan method exist in the literature [23, 31, 41–44]. Models including single nonlinear absorption mechanisms such as pure 2PA [23], higher-order nonlinear absorption [31], and mixed multiphoton absorption [41–43] have been presented. In contrast to single absorption processes, mixed multiphoton absorption is only occasionally observed [45] and measured [46–48]. Non-idealities, such as ellipticity [44] and laser beam quality [49, 50], can obscure interpretation of mixed multiphoton data by changing the shape of the Z-scan curve. For example, beam ellipticity reduces the total signal and can cause asymmetry [44]. Meanwhile, the beam quality factor, M^2, reduces the apparent Rayleigh distance by $1/M^2$ while maintaining the waist [49–51]. Mixed multiphoton absorption is particularly sensitive to such shape changes [41–43]. These effects are not included in the previous models. Thus, we develop a mixed multiphoton absorption model that includes these non-idealities here.

We apply an open aperture Z-scan derivation using an elliptical beam, similar to that presented in Ref [44]. and highlight the differences. We start with Equation 10 for an elliptical Gaussian beam from reference [44]:

$$I_{in}\left[x, y, z, P(t)\right] = \frac{2P(t)}{\pi w_x(z) w_y(z)} \exp\left[-\frac{2x^2}{w_x^2(z)} - \frac{2y^2}{w_y^2(z)}\right]. \tag{A.1}$$

Here, z is the sample position, x and y are the transverse spatial coordinates, $P(t)$ is the instantaneous power as a function of time, and $w_x(z)$ and $w_y(z)$ are the beam widths as a function of the sample position, z. We include the beam quality factor through the width as follows:

$$w_x(z) = \sqrt{w_{x0}^2 + \left(\frac{M_x^2 \lambda_0}{\pi w_{x0}}\right)^2 (z - z_{x0})^2}. \tag{A.2}$$

In this equation, w_{x0} is the beam waist, M_{x2} is the beam quality factor [51], z_{x0} is the location of the waist and λ_0 is the center wavelength. We use a similar expression in the y-direction. We define the ellipticity by w_{x0}/w_{y0} and the astigmatism by $z_{x0}-z_{y0}$. We include 3PA in the attenuation coefficient, defined for a single wavelength by $\alpha(I) = \alpha_0 + \alpha_2 I + \alpha_3 I_2$. Here I is the intensity, and α_0, α_2, and α_3 are the one-, two-, and three-photon absorption coefficients, respectively. Rutile is highly transparent for 800 nm, so we set α_0 to zero. We solve the following ordinary different equation using standard numerical methods along the sample length, L:

$$\frac{dI}{dz'} = -\alpha(I)I. \tag{A.3}$$

Here, z' is the position inside the sample. We solve for each point in x and y at a fixed sample position (z). Then, we integrate over x and y at the entrance and exit of the sample to

calculate the transmittance (power out normalized to power in). It should be noted that by following conventional theory [23], we do not include the effects of self-phase modulation, self-focusing (e.g. filamentation), or dispersion. We model pulsed transmittance using a Gaussian shape, given by $P(t)$, integrated over time using:

$$T(z) = \frac{\int P(t)T[z,P(t)]dt}{\int P(t)\,dt} = \frac{E_{out}(z)}{E_{in}}.$$ (A.4)

In this equation, $T(z)$ is the observed energy transmittance, $T[z, P(t)]$ is the instantaneous power transmittance, and E_{in} and E_{out} are the input and output energies, respectively. We take into account the reflection from the front surface. Numerical methods require that we discretize our parameters including the x- and y-position and time. Consequently, we test for the convergence of all discretization parameters. Additionally, we find excellent agreement between this model and analytical solutions for two- [23] and three-photon absorption [31].

Unless otherwise stated, we fit each data set (multiple Z-scan traces at different powers) using this model to a single set of fit parameters, keeping all others fixed to experimental values. We fit our data using the Levenberg-Marquardt method. Our fit parameters are α_2, α_3, the average z-position of the waist (z_0) and the astigmatism. From this fit, we determine a single value for α_2 and α_3 that describes the Z-scan traces for all irradiances measured.

Acknowledgments